

# *IET Renewable Power Generation*

## **Special Issue Call for Papers**

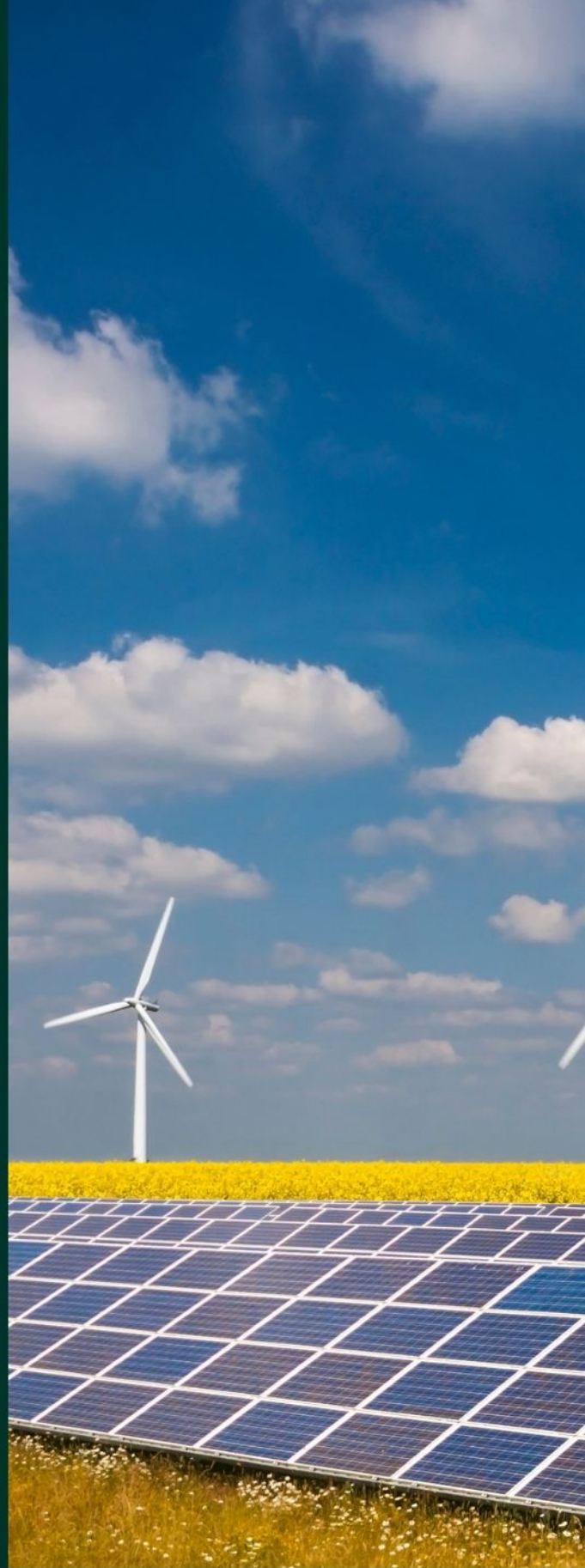
---

**Be Seen. Be Cited.  
Submit your work to a new  
IET special issue**

Connect with researchers and  
experts in your field and  
share knowledge.





Be part of the latest research  
trends, faster.

[Read more](#)



The Institution of  
Engineering and Technology

# Ocean wave power forecasting using convolutional neural networks

Pedro Bento<sup>1,2</sup>  | José Pombo<sup>1</sup>  | Maria do Rosário Calado<sup>1,2</sup>  | Sílvio Mariano<sup>1,2</sup> 

<sup>1</sup> Department of Electromechanical Engineering, University of Beira Interior, Covilhã 6201-001, Portugal (Email: [pedro.bento@lx.it.pt](mailto:pedro.bento@lx.it.pt); [jose.pombo@ubi.pt](mailto:jose.pombo@ubi.pt); [rc@ubi.pt](mailto:rc@ubi.pt))

<sup>2</sup> Instituto de Telecomunicações, Covilhã 6201-001, Portugal

## Correspondence

Sílvio Mariano, University of Beira Interior, Covilhã, 6201-001 Portugal  
Email: [sm@ubi.pt](mailto:sm@ubi.pt)

## Funding information

FCT/MCTES, Grant/Award Number: UIDB/50008/2020; Fundacao para a Ciencia e a Tecnologia, Grant/Award Number: SFRH/BD/140371/2018

## Abstract

Climate change “fuelled” by anthropogenic causes has been identified as the greatest threat faced by societies. In this respect, the roadmap to a “greener” generation mix certainly includes a greater heterogeneity in terms of renewable energy sources. In this regard, one of the leading candidates is ocean wave energy. One of the issues with renewables in general is their unpredictability and variability, as it is crucial to address the subject of wave power forecasting, to facilitate a future market integration. Hence, to tackle this prediction problem, a new approach to short-term wave power forecasting is proposed, based on deep learning capabilities. These highly popular networks were traditionally developed to deal with images (2D data), so the authors discuss all the necessary implementation and design details to employ these networks with 1D input data, to solve a regression-based problem. These case-studies include wave data from three different locations. The proposed approach was tested across all seasons of the year, revealing the suitability to extract the relevant input data dependencies from the time-series. As such, especially for horizons up to 6 h, the proposed approach outperforms other conventional methods.

## 1 | INTRODUCTION

In the ever increasing quest to develop alternative and non-conventional renewable energy technologies to effectively tackle the increased demand for energy, escalating energy prices, and the environmental harms associated with fossil-based electricity production, researchers have made major efforts, over the last few decades, to develop and to facilitate the use of renewable energy sources (RES) [1]. These concerted efforts aim to enrich the increasingly “particoloured” energy portfolio. With this in mind, ocean renewable energy (ORE) stands out as one of the fittest contenders, with densities several times greater than wind and solar energies [2], coupled with virtually endless flows guaranteeing continuous energy availability (relatively high availability and utilization factor), that is, with the possibility to operate ‘24/7’ [3, 4]. These inherent characteristics of wave energy unveil an enormous potential, and several estimates suggest generated electricity figures ranging between 8 and 80 PWh per year [5, 6].

On the other hand, it is important to recognize that development costs, lack of convergence, potential impact on biodiver-

sity, transmission requirements, and above all the (operational) harsh environment has delayed the commercialization and wide adoption of these emerging RES in comparison with more mature technologies [7]. Despite these challenges, the inherent qualities of ocean wave energy, together with the sizeable RD&D investments on wave energy converters, particularly in the EU [8], allow us to anticipate a successful future integration of ORE resources into the grid. Hence, contributing to the ambitious targets in terms of RESs generation share, which the EU estimates to be at least 27% by 2030 and much higher by 2050 [9].

In this foreseeable scenario and following the lead of more mature technologies, predicting the energy production from RES, and in particular wave conditions/wave power, is critical to maintaining a stable electrical grid due to its intermittent and non-dispatchable nature of these generation technologies [9, 10], especially as the amount of energy generated from these sources increases [11]. Additionally, these predictions are also key for project planning, decision-making and risk management of market players [12] and developers. Hence, if wave energy technologies are expected to play a significant role in a future

This is an open access article under the terms of the [Creative Commons Attribution](https://creativecommons.org/licenses/by/4.0/) License, which permits use, distribution and reproduction in any medium, provided the original work is properly cited.

© 2021 The Authors. *IET Renewable Power Generation* published by John Wiley & Sons Ltd on behalf of The Institution of Engineering and Technology

cleaner energy mix, then it is crucial to have accurate estimates of the potential energy production in order to lay the foundations for suitable wave energy converters [13, 14].

However, the benefits of developing accurate forecasting models go far-beyond the latter, and the list includes aquaculture industry, optimised shipping routes, nautical sports, military operations etc [10]. Consequently, ocean wave forecasting essentially focus on the challenging task of predicting characteristic wave heights and periods using readily available weather conditions [15].

The future role of wave energy technologies coupled with all the different applications of wave energy forecasting are the reason behind an increasing number of works in this field. This follows a broader trend in the renewable forecasting literature, which is attributed to the intense worldwide renewable integration efforts [16]. It also constitutes the main motivation of the presented work.

One literature survey reveals three conventional categories of methods to perform this task, namely: i) numerical approaches primarily centered on wave energy-balance relationships [17]. For example, authors in [18, 19] used the popular wave numerical model WAVEWATCH III (WW3) to perform the forecasting task of ocean wave energy related variables; other popular choices are simulating wave nearshore (SWAN) and community climate system model (CCSM4) models [15, 18]. Even though wave numerical models offer a good accuracy, they tend to be computationally expensive, thereby, opening path for machine learning (ML) approaches [10, 15]. ii) Statistical methods such as regression, Box–Jenkins method applying auto regressive moving average (ARMA) [20] and auto regressive integrated moving average (ARIMA) models, exponential smoothing, among others are a common choice to solve a time-series forecasting task. However, a common downside is the difficulty to capture non-linear data patterns [21]. iii) Soft-computing approaches are amongst the trendiest options due to their ability of efficiently mapping large datasets and deal with non-linearities in the predicted and auxiliary time-series. The list includes trendy ML and deep learning (DL) based methods, fuzzy logic, expert systems, decision trees, genetic algorithms, and hybrid approaches [13, 22].

A particular highlight can be given to ML approaches, which overcome several shortcomings of traditional data analysis techniques, thus providing accurate and efficient methods for predicting ocean related variables [23]. In this field, artificial neural networks (ANNs) [24, 25] and support vector machines (SVMs), multi-layer perceptron (MLP) [10, 15], non-linear autoregressive network with exogenous inputs (NARX) [17], recurrent neural networks (RNNs) [26], random forests (RF) [27], and extreme learning machine (ELM) [28], are among the most common choices used in forecasting.

An example of a hybrid approach is given in [29], where a genetic fuzzy system built on a three- staged algorithm is used to estimate significant wave height and energy flux. In another instance, a hybrid grouping genetic algorithm—ELM approach is proposed in [30]. Alternatively, a wavelet and neural network hybrid model was developed in combination with empirical orthogonal function analysis to better the performance of tra-

ditional ANNs [31]. In another instance a comparison between single and multi-layered RNN, LSTM, and seq-to-seq networks is conducted in [32], and in [33] ocean wave height is also predicted using a LSTM network, proving its superior accuracy in comparison with a MLP network, SVM and RF.

In the wake of all these successful approaches where ML and DL are employed to predict all sorts of wave energy related data, this paper presents and discusses a new DL approach based on convolutional neural networks (CNNs or ConvNets) to tackle a research gap, where better short-term wave power forecasting approaches are being searched. In addition, we can summarize the main contributions as follows:

- In the wake of the developments of DL, a CNN is introduced for the task of short-term wave power flux forecasting by exploiting its advantage of not requiring an exhaustive input pre-processing stage.
- A tailored dual layered CNN architecture was designed to accommodate the different specificities of the 1D datasets, in order to extract the most relevant characteristics of the time-series.
- Wave data from 3 different datasets were analysed and used to validate the proposed approach for a variety of prediction steps-ahead.
- Direct and indirect results analyses reveal an encouraging forecasting performance, especially between 1 h to 6 h in all case-studies. This highlights the broad scope of application of the proposed approach.

The rest of the paper is organised as follows: Section 2 provides a brief theoretical background of the most important sea state parameters and is about how the wave power is estimated, followed by the illustration and relevant statistics of the wave data used as case-studies in this work. Section 3 describes the methodology, starting with the CNN fundamentals and ending with the key data selection implementation details of the proposed CNN. Subsequently, Section 4 discusses the testing procedure, error metrics, and results. Lastly, Section 5 outlines the main conclusions of this work.

## 2 | WAVE POWER AND SEA STATE PARAMETERS

The main considerations about sea state parameters and wave power required to understand the predictable variable in the short-term wave power forecasting, as well as the auxiliary associated variables, are presented in this section. Afterward, the wave data employed in this work is illustrated together with the main statistics.

### 2.1 | Wave power estimation

In the last few decades, climate models and particularly wave models were refined to produce a greater understanding of the different physical interactions responsible for wave

**TABLE 1** Statistics of the different wave power datasets [ $\text{kWm}^{-1}$ ]

Buoy ID/stats	Mean	Min	Max	St. dev <sup>a</sup>	Skew	Kurt
41048	18.19	0.72	461.62	24.93	3.93	28.44
42056	6.27	0.25	184.45	8.08	4.88	50.32
44014	12.42	0.39	261.90	19.73	4.33	29.42

<sup>a</sup>St. dev - Standard Deviation.

phenomena, providing useful knowledge for public and private entities to better monitor and explore ocean resources, for example, when we explore the potential of wave energy converters in certain sea state conditions. To achieve this goal, meteorological, sea, and atmospheric agencies across the globe, such as National Oceanic and Atmospheric Agency (NOAA), have greatly expanded scalar buoy and nautical radar measurements of ocean waves (wind generated) to better study the sea state spectral parameters estimated from both sensors [34].

In this work, we are solely interested in the set of sea state parameters from where it is possible to derive a wave power expression. So, we define the mean transport rate of the wave energy through a vertical plane of unit width, parallel to a wave crest, as the wave energy flux or more broadly, wave power,  $J$  [ $\text{kWm}^{-1}$ ] (1). And in deep water conditions, that is, where the water depth is larger than half the wavelength, the same can be computed as follows [35]:

$$J = \frac{\left(\frac{\rho g^2}{64\pi} H_{m0}^2 T_e\right)}{1000} \approx 0.491 (H_{m0}^2 T_e), \quad (1)$$

where  $H_{m0}$  is the significant wave height;  $T_e$  the wave energy period;  $\rho$  the saltwater density; and  $g$  the acceleration due to gravity. When the significant wave height is given in metres and the wave period in seconds, the result is the wave power in kilowatts (kW) per meter of the wave front length.

## 2.2 | Wave data

In this work, three different hourly datasets will be used to evaluate the forecasting performance of CNNs. These comprise a set of quality-controlled buoy measurements gathered by the US National Data Buoy Centre (NDBC), spanning between January 2007 and April 2010. The respective buoy IDs are: 41048 in the West Bermuda; 42056 Yucatan Basin between the Caribbean Sea and the Gulf of Mexico; 44014 Virginia Beach, Virginia. The focus of this work will be to predict the wave power or wave energy flux,  $J$ , however, the variables of interest to assemble the input data also include  $H_{m0}$ ,  $T_e$  and windspeed,  $v$ .

With this regard, it is important to analyse the time-series statistics, and therefore Table 1 is presented, showing the mean, upper and lower occurrences, standard deviation, and the shape related statistics, kurtosis, and skewness.

These stats show a diversified scenario between datasets, which will help validate the forecasting performance over a wide range of sea state conditions. However, a commonality between the datasets is the greater standard deviations with highly right-

skewed data and with a leptokurtic distribution. Moreover, the use of these specific datasets allows us to benchmark the obtained results against several conventional approaches also considered in [25, 36].

A visual characterisation of the energy density in terms of significant wave height and energy period is shown in Figure 1 for all the datasets.

This allows us to clearly see the variability of sea state conditions, the absolute frequency of different sea state conditions (pair  $H_{m0}$  and  $T_e$ ), as well as the associated (available) wave density and power, thus validating the representativeness of the considered datasets.

## 3 | METHODOLOGY: THEORY AND IMPLEMENTATION

As the name suggests, this section introduces the important CNN design and implementation details, as well as the different stages of the proposed forecasting approach, starting with the fundamentals of CNN topology, followed by the required adaptations to use it in the context of one-dimensional space data for a prediction-based problem, detailing the assemble stage of the input training and target samples.

### 3.1 | Convolutional neural networks

The development of DL approaches has expanded past conventional classification problems, and the vast landscape of ML and DL techniques are being applied across various research fields. As we saw in the Introduction, the same is valid for wave power forecasting, where these approaches are gaining wide traction, much due to their ability to model complex non-linear relationships between sets of input and output data.

With this respect, CNNs are one of the most promising and popular DL approaches [37, 38]. Originally conceived for large-scale image classification, where they have been tremendously successful [39], CNNs are a type of bio-inspired feed-forward type of ANN architecture that eliminates the need for manual feature extraction [37], and is particularly tailored for analysing and finding patterns in two-dimensional data. However, the application scope of CNNs extends beyond image data, and it has been successfully applied in signal processing and time-series analysis (1D data), audio analysis (2D data) and video classification (3D data) etc. CNNs consist of a sequence of layers and its core building blocks are the Convolutional (ConvLayer) and Pooling (subsampling) layers which have different roles during the training process, as illustrated in Figure 2 [38, 40].

Convolution layers are composed by neurons with weights and biases which are then continuously updated (each training epoch), to minimize a loss function. However, for a given hidden layer the value of the weights and biases is the same for all neurons, which is a major contrast with the standard fully connected networks. Another major difference is that instead of a fully connected architecture, connections are local in space (across the width and height of the input volume) but always

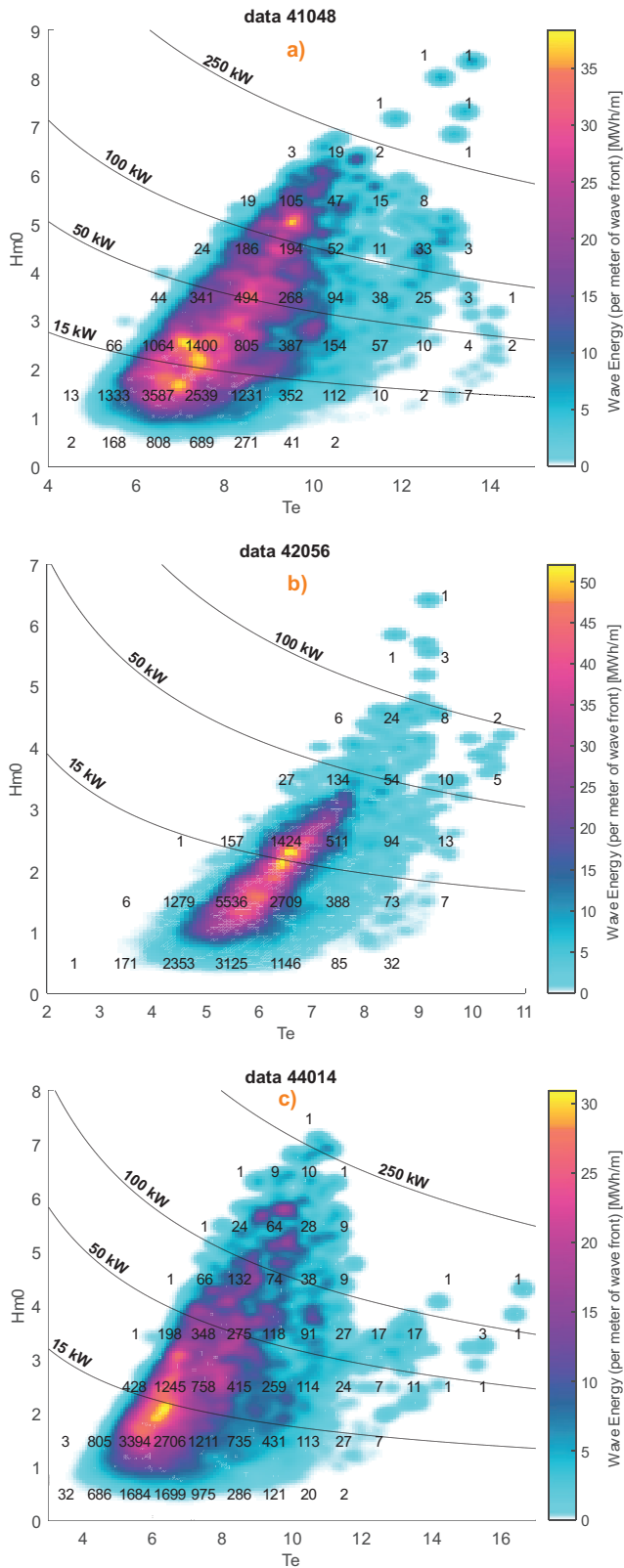


**FIGURE 1** Kernel joint probability density estimation of the collected observations. The colour scale represents the wave energy per metre of wave front (in MWh/m). The numbers within the graphs indicate the occurrence of sea states (in number of hours per year) and the isolines refer to the wave power  $J$  (in kW) (a) Buoy ID: 41048, (b) Buoy ID: 42056, (c) Buoy ID: 44014

full along the entire depth of the input volume, that is, there is an asymmetry in how spatial and depth dimensions are handled. The spatial extent of the local connection is called receptive field (inspired in the biological visual cortex) or filter size.

So, a ConvLayer contains an entire set of filters, each one producing an individual activation map which is stacked along the depth dimension resulting in the output volume, that is, each filter is convolved across the width and height of the input volume. These (learnable) filters are sparse and shared across the entire input and are adjusted during the training process, in order to be activated when certain features are detected. Thus, we can define in Equation (2) the output result/ feature map  $y_k^{(m)}$  from the convolution operation that occurs in an arbitrary ConvLayer  $k$ , between an input from an arbitrary layer  $k-1$ ,  $x_{k-1}^{(c)}$ , and the  $m^b$  filter of such channel  $c$  in layer  $k$ ,  $W_k^{(c,m)}$ , followed by the added bias term  $b_k^{(c)}$ ,  $f_j$  being the chosen activation function [41].

$$y_k^{(m)} = f_j \left( \sum_{c=1}^C W_k^{(c,m)} * x_{k-1}^{(c)} + b_k^{(c)} \right). \quad (2)$$

Additionally, two common operations performed that influence the outcome of the convolution between the input and the filter/kernel are padding and striding. The first, padding  $p$ , defines the number of “pixels” added to the input (extremities), and it avoids a sizeable input shrinking and reduces the discrepancy in the treatment of central versus corner “pixels”. The second, stride  $s$ , describes what is the step taken across spatial dimensions while consecutively convoluting filters with the inputs. An increased stride will lead to a reduced output dimension, which is the opposite result of padding. So, the output of each convolved input volume is used as the input to the next hidden layer, and for an arbitrary input size  $[n_b \times n_w \times n_c]$  and filter size  $[f_1 \times f_2]$ , the generalized output dimensions of a ConvLayer with  $n_f$  filters are:

$$\left[ \left( \frac{n_b + 2p - f_1}{s} + 1 \right) \times \left( \frac{n_w + 2p - f_2}{s} + 1 \right) \times n_f \right] \quad (3)$$

where subscripts  $b$ ,  $w$  and  $c$  represent height, width, and channels (depth), respectively.

In turn, a pooling layer, is responsible for a non-linear downsampling of the input volume, thereby, reducing the number of learnable parameters and hence speed up the computation cost. To execute the downsampling, a max or average pooling layers are commonly used, and in the same fashion as ConvLayers, pooling layer’s hyperparameters also include kernel size, stride, and padding. Thus, the output dimensions are obtained similar to Equation (3), with the exception of depth that retains the size of the input volume that is forward to the pooling layer. Other common hidden layers in a ConvNet are normalization layers, that is, which normalize the output of the previous layers to improve the batch learning process; flatten layers, as the name suggests, flatten/collapse the input dimensions  $[n_b \times n_w \times n_c]$  to

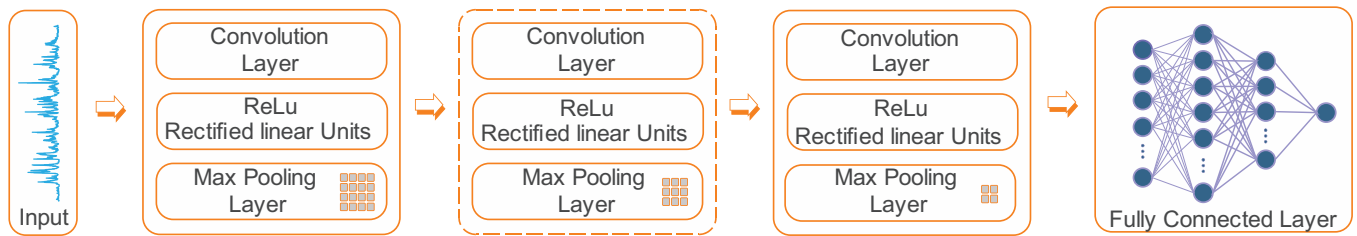


FIGURE 2 Convolutional neural network (CNN or ConvNet) architecture

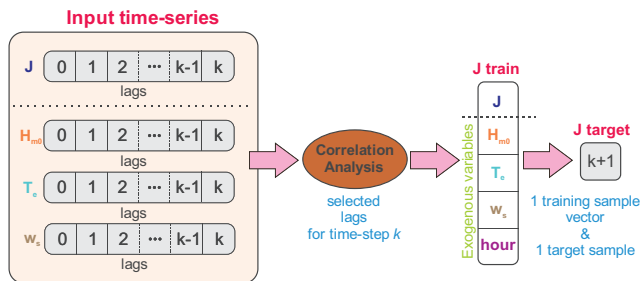


FIGURE 3 Wave pre-processing and input data selection

a one-dimensional output, allowing the transition from convolution layers to a traditional dense/fully connected layer. As for the output layer, it can be either categorical or continuous.

### 3.2 | Proposed methodology

In order to implement a CNN capable of predicting wave power for different forecasting horizons, we start the process by analysing the partial autocorrelation magnitudes (PACF), as well as the Pearson correlation, for the forecasted variable  $J$ , and the exogenous inputs  $H_m(t)$ ,  $T_e$  and  $w_s$ . Besides, the hourly index of the corresponding target output  $J$  is also fed into the CNN to provide some account of the observed daily seasonalities. Since even though a CNN does not require a manual feature selection, due to its DL capabilities, it is still important to only feed input samples and parallel input variables with a significant correlation. In this work, a threshold level of 0.05 was considered. This avoids a more time-consuming training task and reduces the potential length (height) of the input samples, which can impact the kernel size. An illustration of this pre-processing and data selection stage is shown in Figure 3, where after performing a correlation analysis (auto and partial correlation) of the different time-series, the correspondent training and testing samples are assembled with its pairing target data.

Furthermore, it is important to notice that although CNNs are traditionally employed with 2D data, as we have seen in Section 3.1, they can also be used to model univariate time-series. The difference resides in the kernel size, which has the same width as the time-series, while the height may differ. In this way, the filter moves only across one dimension. In the event of a multivariate time-series, as is the case in this work, the several

inputs are fed in parallel, analogously to the different colour channels in the 2D data, meaning they are treated fully along the depth dimension, but locally in terms of spatial dimensions. To sum up, a 1D CNN completes a 1D convolution operation and is followed by a dimensionality reduction, combining the feature extraction, transformation, data fusion, and classification steps into one framework [42].

So, after having assembled the input data with exogenous variables, in the form of input samples with the corresponding target output, we moved on to building the forecasting CNN architecture. As can be seen in Figure 4 it has two ConvLayers, which is a preferred option over a single ConvLayer when dealing with long input sequences. The filters of these hidden layers will be activated, to signal certain input features. Then, the customary non-linear activation function rectified linear unit (ReLU) is called to map the convolution operations. This function has the particularity of only keeping the positive values (activated features), since negative values are set to zero. After that, two max pooling layers are used to condense the output (feature maps) of ConvLayers, maintaining only the most salient values. These hidden layers are followed by a flatten layer to compress the output volume to a single dimension vector. In turn, this will be the input to a dense (fully connected) layer, whose task will be to interpret the features extracted by the convolution part of the architecture and to produce a single valued output. The dense layer also has a dropout rate of 20%, in order to improve its generalization capabilities.

To implement the aforementioned CNN, the authors have resorted to Python 3.8.7, using the TensorFlow and Keras DL libraries, and simulations were performed on Windows 10® with an Intel Xeon E5-1620 v4 CPU.

Additionally, regarding the input data size, we have considered the previous 30 days before the test week, to assemble the training input samples. This value enables a compromise between diversity in the training samples and reasonably recent data, that is, a batch of roughly 720 samples, with a validation ratio of 15%. With these training and validation samples, the ConvNet will learn to map the input sequences, and each layer will be capable of learning to identify different features. To achieve this goal, the weights and biases are learned by minimizing the chosen loss function (4), which in this work was the mean squared error (MSE):

$$\min_w MSE = 1/N \sum_{s=1}^N (z_s - \hat{z}_s), \quad (4)$$

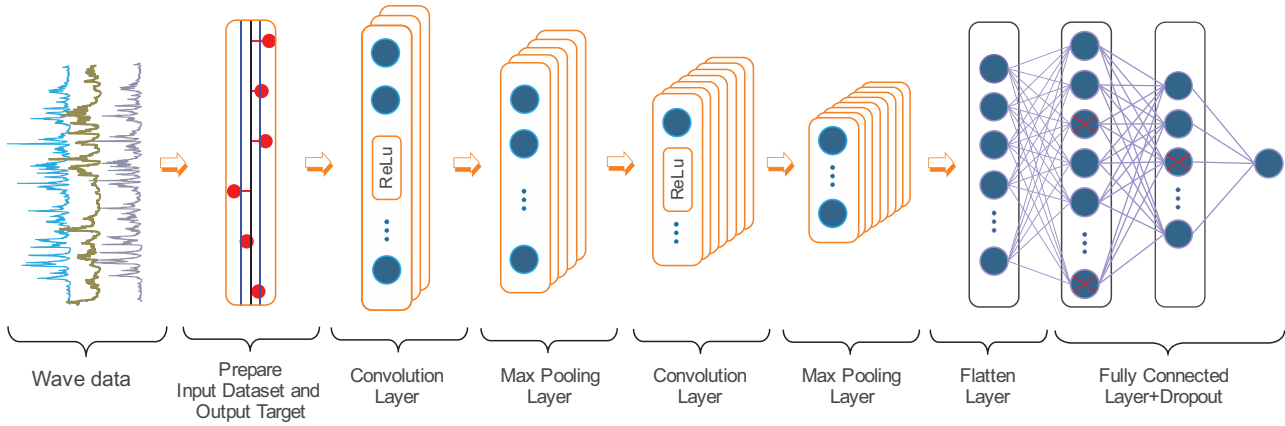


**FIGURE 4** Proposed methodology (overview): CNN architecture fed with several 1D wave input data

**TABLE 2** Forecasting: Testing dates

Buoy ID/ season	WinterWeek	SpringWeek	SummerWeek	FallWeek
41048	07/02/08-13-02-08	01/05/08-07/05/08	12/08/08-16/08/08	22/10/08-28/10/08
42056	07/02/08-13-02-08	15/05/08-21/05/08	19/08/08-25/08/08	12/11/08-18/11/08
44014	31/01/08-06-02-08	08/05/08-14/05/08	22/07/08-28/07/08	29/10/08-05/11/08

where  $W$  represents the learnable CNN weights,  $N$  is the batch size,  $\hat{z}_x$  is the CNN output in this epoch, and  $z_x$  is the targeted output response. With respect to the task of training the CNN, the adaptive moment estimation (Adam) was chosen. This stochastic optimizer computes the individual adaptive learning rates for different parameters from estimates of first and second moments of the gradients, for each learning epoch [43].

## 4 | RESULTS

The proposed methodology is used to perform the short-term wave power forecast,  $J$ , for the three datasets, considering lead times of 1, 2, 3, 6, and 12 h.

For validation reasons, four weeks of testing are considered, one week per calendar season of the year (northern hemisphere), which ensures that the results are not tied to a specific seasonality or trend. The testing dates for each dataset can be seen in Table 2.

Additionally, for each testing date, the CNN model was evaluated (trained and tested) for 15 times, that is, 15 runs; this allows us to have a more solidified conclusion about the model performance. To evaluate the forecasting performance we employed common error metrics, namely the correlation coefficient ( $r$ ), mean absolute percentual log-difference error (MAPE-log), and root mean squared error (RMSE), as seen below in Equations (5)–(7).

$$r = \frac{\sum_{i=1}^{N_s} [(p_i - \bar{p}) \cdot (o_i - \bar{o})]}{\sqrt{\sum_{i=1}^{N_s} (p_i - \bar{p})^2 \cdot \sum_{i=1}^{N_s} (o_i - \bar{o})^2}}, \quad (5)$$

$$\text{MAPE log [\%]} = 100 \cdot \frac{\sum_{i=1}^{N_s} |\log p_i - \log o_i|}{N_s}, \quad (6)$$

$$\text{RMSE} [kW/m] = \sqrt{\frac{\sum_{i=1}^{N_s} |p_i - o_i|}{N_s}}, \quad (7)$$

where  $N_s$  is the number of testing samples;  $\bar{p}$  and  $p_i$  are the average (for all  $N_s$  samples) predicted wave power and the predicted wave power at time-step  $i$ , respectively; and  $\bar{o}$  and  $o_i$  are the average real wave power and the real wave power at time-step  $i$ , respectively.

After completing the simulations, the mean forecasting results ( $r$ , MAPE log and RMSE) for the three datasets, for each forecasting horizon, is compiled (see Tables 3–5). Besides, Tables A.1–A.3 in the Appendix present the best individual error metrics for each buoy, test week, and forecasting horizon.

So, by analysing the tables we can see that naturally the forecasting accuracy decreases as the forecasting horizon increases, with error metrics, in terms of RMSE, increasing in comparison with the previous lead times, in the order of  $\approx 15\%$ – $20\%$  (between 1 and 2 h),  $\approx 18.0\%$ – $19\%$  (between 2 and 3h),  $\approx 25\%$ – $50\%$  (between 3 and 6 h), and  $\approx 35\%$ – $57.4\%$  (between 6 and 12). Moreover, there is an obvious connection between the prediction accuracy and the season of the year, where the CNN testing is being conducted since, as we saw in Table 1, there is a great standard deviation in the data, with significant higher wave power during the winter and fall seasons.

Commencing with buoy data 41048, Table 3 reveals a relatively uniform accuracy across all seasons, with the exception of 12 h horizon, with error metrics of 0.97–0.29 in terms of  $r$ ,

**TABLE 3** Forecasting errors: Buoy 41048 (mean results)

For hor/ season	WinterWeek			SpringWeek			SummerWeek			FallWeek		
	<i>r</i>	MAPElog	RMSE	<i>r</i>	MAPElog	RMSE	<i>r</i>	MAPElog	RMSE	<i>r</i>	MAPElog	RMSE
1 h	0.96	14.40	6.22	0.95	14.34	4.51	0.94	15.48	3.04	0.97	11.12	3.19
2 h	0.95	17.57	8.11	0.94	16.11	4.19	0.92	17.84	3.43	0.95	13.98	3.91
3 h	0.93	21.49	9.36	0.92	18.82	5.18	0.89	20.29	4.01	0.92	17.16	4.92
6 h	0.92	28.19	8.92	0.72	28.30	6.38	0.80	33.26	5.68	0.82	31.68	8.38
12 h	0.85	38.91	12.32	0.29	52.81	12.66	0.69	39.05	6.88	0.54	51.84	19.75

**TABLE 4** Forecasting errors: Buoy 42056 (mean results)

For hor/ season	WinterWeek			SpringWeek			SummerWeek			FallWeek		
	<i>r</i>	MAPElog	RMSE	<i>r</i>	MAPElog	RMSE	<i>r</i>	MAPElog	RMSE	<i>r</i>	MAPElog	RMSE
1 h	0.97	10.10	0.78	0.95	10.05	0.27	0.97	12.31	0.27	0.94	12.18	2.52
2 h	0.95	12.88	0.95	0.93	12.65	0.34	0.95	15.60	0.34	0.93	15.43	2.85
3 h	0.93	16.01	1.13	0.90	15.45	0.42	0.95	14.66	0.39	0.90	18.74	3.37
6 h	0.87	22.33	1.47	0.75	24.67	0.69	0.87	27.52	0.67	0.84	26.94	4.61
12 h	0.67	31.60	2.21	0.40	45.08	1.70	0.84	24.15	0.78	0.69	41.76	7.02

11.12%–52.81% in terms of MAPE log and 3.19–19.75  $\text{kW}/m$  in terms of  $e_3$ . These results are in line with the regression and neural net models overall means in [36], the same dataset, with the exception being the 12 h horizon, where the accuracy falls by  $\sim 50\%$  in terms of RMSE. Therefore, demonstrating the need to use combined models in this dataset, that is, it would heavily benefit from the physical model “guidance”. With regards to the best achieved values, Table A.1 shows gain between 5 and 10%. Now by analysing the buoy 42056, error metrics vary in the range 0.97–0.40 in terms of  $r$ , 10.05%–45.08% in terms of MAPE log and 0.27–7.02  $\text{kW}/m$  in terms of  $e_3$ . In this case, we see an improvement in all forecasting horizons, when we compare them with the ones obtained by the physical models, regression, and neural network. As for buoy 44014 results, the error metrics average is in the range 0.95–0.60, 17.6%–63% and 6.24–15.22  $\text{kW}/m$ , for  $r$ , MAPE log and RMSE, respectively.

In turn, the distribution (box-and-whisker plots) of the error metrics during the runs was also analysed, considering all seasons, and forecasting horizons, and Figure 5 is presented to

demonstrate the behaviour of the CNN during the runs for buoy data 41048. It is revealed that the employed ConvNet model presents a generally stable forecasting accuracy (a smaller interquartile range), certainly for the first 3 horizons; then from 6 h onward the error spread increases, which translate an added difficulty in extrapolating relevant information from the available input dataset. Additionally, there were no significant outliers. The corresponding figures for the remaining datasets are introduced in the Appendix, and a similar picture is painted in Figures A.1 and A.2.

For further comparison purposes, some ML conventional forecasting techniques were implemented using the same input data. First, a common fully connected NN was selected to benchmark the obtained results. The NN was configured with 32 neurons in the hidden layer, a hyperbolic tangent sigmoid as the chosen activation function, and it is trained using the Levenberg–Marquardt method (maximum number of 1000 iterations) with a training to validation ratio of 80%. Second, we choose a generalized radial basis function network (RBNN)

**TABLE 5** Forecasting errors: Buoy 44014 (mean results)

For hor/ season	WinterWeek			SpringWeek			SummerWeek			FallWeek		
	<i>r</i>	MAPElog	RMSE	<i>r</i>	MAPElog	RMSE	<i>r</i>	MAPElog	RMSE	<i>r</i>	MAPElog	RMSE
1 h	0.97	13.80	5.84	0.97	19.21	14.96	0.91	15.79	0.43	0.93	21.46	3.73
2 h	0.94	18.63	6.62	0.93	26.09	18.19	0.84	21.72	0.58	0.88	29.03	4.98
3 h	0.93	23.58	6.68	0.93	35.14	20.51	0.73	26.79	0.75	0.84	39.05	5.94
6 h	0.84	39.52	8.91	0.86	52.23	28.95	0.53	33.27	0.96	0.72	57.20	8.63
12 h	0.68	57.95	10.64	0.80	68.79	36.15	0.41	43.29	1.20	0.51	84.89	12.89



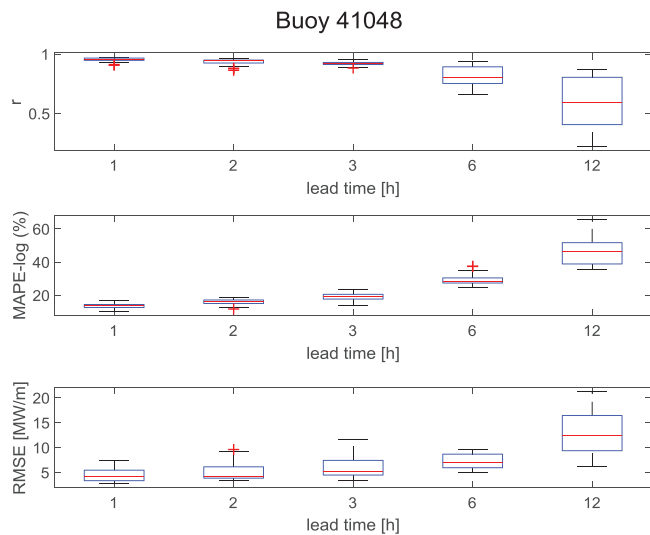


**FIGURE 5** Box plots of the error metrics distributions, considering all forecasting horizons (buoy 41048)

with a maximum number of 1000 neurons, in order to fit the radial basis neurons with a spread of 1 to reproduce the training pattern with a good compromise (to avoid overfitting). The last comparative method was a Support Vector Machine regression model, which is also a common ML method employed to continuous data and regression analysis. In this work, we used a predefined third-degree polynomial approximation as a kernel function.

The resulting error metrics of this direct comparison of different ML forecasting methodologies can be seen in Tables A.4–A.6, which for convenience purposes were placed in the Appendix. The results for the buoy data 41048 reveal a superior performance of the proposed approach, in almost all metrics and horizons (highlighted in bold). The exceptions occurred for longer horizons (6 and 12 h) in terms of MAPE log and RMSE for the summer and fall weeks (where the conventional NN and RB with the same input data achieved slightly better results). With regard to buoy data 42056, a similar picture was that the proposed approach consistently outperforms the other methods, with the exception being typically for longer horizons in the summer test week. Finally, the error metrics for buoy data 44014 are no exception to the rule, confirming a 2% to 11% better average accuracy, and the proposed methodology is only outperformed by the RBNN, particularly in the longer horizons, and more so in terms of MAPE log.

A graphical representation of the short-term wave forecasting is given in Figure 6, where we can see the real and predicted wave power (left axis), as well as the absolute error (right axis), for all the considered forecasting horizons, regarding buoy data 41048 (spring testing week).

Additionally, Figure 7 is also introduced to illustrate the results of the direct comparison between ML methodologies made in Tables A.4–A.6. It can be visually confirmed that the proposed methodology forecast resembles the real wave power the most.

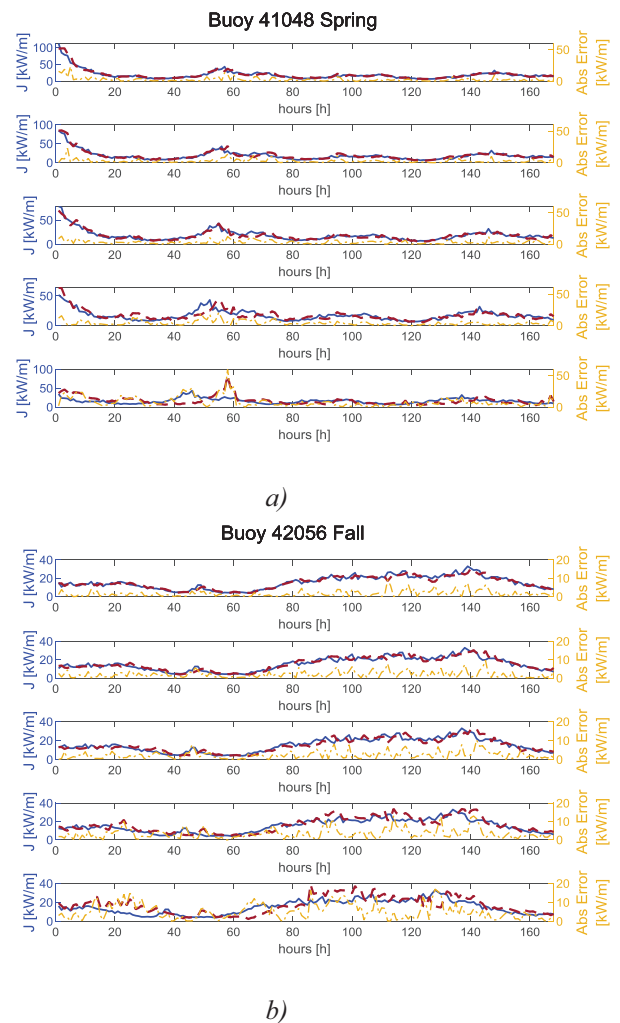


**FIGURE 6** Test results illustration for all horizons: Actual and forecasted wave power flux,  $J$ , respectively, blue solid line and maroon dashed line (left axis) and absolute error, canary yellow dot-dashed line (scaled right axis) ample graph with blue (dotted), green (solid) and red (dashed) lines (a) Buoy 41048 Spring Week, (b) Buoy 42056 Winter Week

## 5 | CONCLUSION

With the advent of DL, researchers and industry have shifted its focus to use these tools for data analysis and features extraction. So, following this path, this work proposes the use of ConvNets for short-term wave power forecasting. These biologically inspired networks have been successfully applied to traditional categorical problems concerning 2D data. However, its distinct nature, where there is sparsity of connections, that is, local connections along the width of the datasets (1D data), makes them interesting to explore and access its potential. Further, a recent day's input data selection, with the auxiliary PACF contributing to feed only relevant wave power time-steps in the input samples, is used to avoid even larger input datasets, which would impact the simulation time, and almost certainly provide irrelevant data. Moreover, the paper also presents the background and considerations that led to the design of this specific CNN model, since many other configurations would be possible.

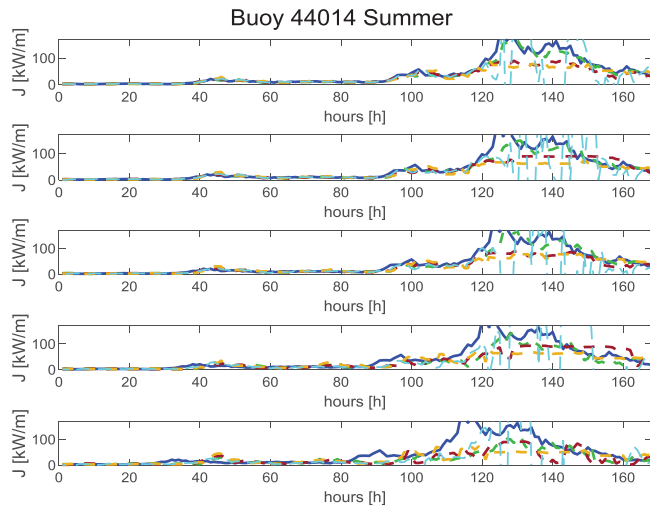


**FIGURE 7** Test results illustration for all horizons: Actual wave power flux,  $J$ , blue solid line; and forecasted wave power flux by CNN (green dashed line), NN (maroon red dashed line), RBNN (canary yellow dashed line) and SVR (cyan dashed line), respectively, and wine dashed line (left axis)

The effectiveness of the proposed method was evaluated in three different case-studies, from NDBC buoy measurements on different sites. The proposed approach is versatile, proving the viability of CNNs, avoiding the need for time-consuming data pre-processing mechanisms. Numerical results reveal good performances, especially for horizons between 2 h and 6 h, where the CNN model can sometimes be quite fitting with a relatively small input training set ( $\sim 30$  days), meaning, average accuracies across all seasons ranged from  $\approx 11\%$  to  $\approx 30\%$ . As for the furthest forecasting horizon, the CNN model was sometimes unable to perform as well, which is normal in non-combined models, that is, without information from a physical (numerical models).

A possible future work will consider different hyperparameter fine-tuning, with different ConvNet architectures being evaluated, that is, different number of ConvLayers and pool Layers, different filter sizes, as well as the use of a lengthier input training with different combinations of exogenous variables, to gauge the DL generalization capabilities, evaluating the potential to improve the proposed CNN methodology.

## ACKNOWLEDGEMENTS

This work is funded by FCT/MCTES through national funds and when applicable co-funded EU funds under the project UIDB/50008/2020. Furthermore, Pedro Bento gives his special thanks to the Fundacao para a Ciencia e a Tecnologia (FCT), Portugal, for the Ph.D. Grant(SFRH/BD/140371/2018). Finally, the authors would like to express their appreciation to Doctor Jean Raymond Bidlot for providing the data.

## NOMENCLATURE


$\hat{z}_s$	CNN output
$w_s$	windspeed
$H_{m0}$	significant wave height
$N_s$	number of testing samples

$T_e$	wave energy period
$W_k^{(c,m)}$	filter weights (ConvLayer neurons)
$b_k^{(c)}$	bias term (ConvLayer)
$f_1 \times f_2$	filter size (window)
$f_j$	activation function evaluation
$n_b$	input height (spatial dimension)
$n_c$	number of input channels (depth)
$n_f$	number of filters
$n_w$	input width (spatial dimension)
$\bar{o}$	average real wave power (all time-steps)
$o_i$	real wave power at time-step $i$
$\bar{p}$	average predicted wave power (all time-steps)
$p_i$	predicted wave power at time-step $i$
$x_{k-1}^{(c)}$	input ConvLayer
$y_k^{(m)}$	output ConvLayer
$z_s$	CNN target output
MAPE – log	mean absolute percentual log-difference
MSE	mean squared error
RMSE	root mean square error
$J$	wave energy (flux)
$N$	batch size (CNN train)
$W$	generic learnable weights
$c$	arbitrary input channel (CNN)
$g$	gravity acceleration
$i$	time-step (sample)
$k$	arbitrary ConvLayer (CNN)
$m$	arbitrary ConvLayer filter (CNN)
$r$	correlation coefficient
$\rho$	Saltwater (volumetric mass) density CNN output

## ORCID

Pedro Bento  <https://orcid.org/0000-0002-9102-7086>

José Pombo  <https://orcid.org/0000-0002-8727-0067>

Maria do Rosário Calado  <https://orcid.org/0000-0002-5206-487X>

Silvio Mariano  <https://orcid.org/0000-0002-6102-5872>

## REFERENCES

- Jahanshahi, A., et al.: Delphi-based prioritization of economic criteria for development of wave and tidal energy technologies. *Energy* 167, 819–827 (2019)
- Mendes, R.P.G., Calado, M.R.A., Mariano, S.J.P.S.: Wave energy potential in Portugal—Assessment based on probabilistic description of ocean waves parameters. *Renewable Energy* 47, 1–8 (2012)
- European Union: Ocean Energy: Promising new technologies to help Europe achieve its ambitious climate goals | H2020 | Results Pack | CORDIS | European Commission. <https://cordis.europa.eu/article/id/422014-ocean-energy-promising-new-technologies-to-help-europe-achieve-its-ambitious-climate-goals>. Accessed December 2020
- Muzathik, A.M., et al.: Wave energy potential of peninsular Malaysia. *ARPN J. Eng. Appl. Sci.* 5(7), 11–23 (2010)
- Melikoglu, M.: Current status and future of ocean energy sources: A global review. *Ocean Eng.* 148, 563–573 (2018)
- IRENA (2020): Innovation Outlook: Ocean Energy Technologies. International Renewable Energy Agency, Abu Dhabi (2020)

7. Johnson, B., Cotilla-Sanchez, E.: Estimating the impact of ocean wave energy on power system reliability with a well-being approach. *IET Renew. Power Gener.* 14(4), 608–615 (2020).
8. Magagna, D., Uihlein, A.: Ocean energy development in Europe: Current status and future perspectives. *Int. J. Mar. Energy* 11, 84–104 (2015).
9. Widén, J., et al.: Variability assessment and forecasting of renewables: A review for solar, wind, wave and tidal resources. *Renewable Sustainable Energy Rev.* 44, 356–375 (2015)
10. James, S.C., Zhang, Y., O'Donncha, F.: A machine learning framework to forecast wave conditions. *Coastal Eng.* 137, 1–10 (2018)
11. Sweeney, C., et al.: The future of forecasting for renewable energy. *WIREs Energy Environ.* 9(2), e365 (2020)
12. O'Donncha, F., et al.: Ensemble model aggregation using a computationally lightweight machine-learning model to forecast ocean waves. *J. Mar. Syst.* 199, 103206 (2019)
13. Avila, D., et al.: Forecasting of wave energy in Canary Islands based on artificial intelligence. *Appl. Ocean Res.* 101, 102189 (2020)
14. Mousavi, S.M., et al.: Deep learning for wave energy converter modeling using long short-term memory. *Mathematics* 9(8), 871 (2021)
15. Feng, X., et al.: A multi-layer perceptron approach for accelerated wave forecasting in Lake Michigan. *Ocean Eng.* 211, 107526 (2020)
16. Hong, T., et al.: Energy forecasting: A review and outlook. *IEEE Open Access J. Power Energy.* 7, 376–388 (2020)
17. Desouky, M.A.A., Abdelkhalik, O.: Wave prediction using wave rider position measurements and NARX network in wave energy conversion. *Appl. Ocean Res.* 82, 10–21 (2019)
18. Bell, R., Kirtman, B.: Seasonal forecasting of winds, waves and currents in the North Pacific. *J. Oper. Oceanogr.* 11(1), 11–26 (2018)
19. Zheng, C.W., et al.: Numerical forecasting experiment of the wave energy resource in the China Sea. *Adv. Meteorol.* 2016, 1–12 (2016)
20. Jeon, J., Taylor, J.W.: Short-term density forecasting of wave energy using ARMA-GARCH models and kernel density estimation. *Int. J. Forecasting* 32(3), 991–1004 (2016)
21. Wang, H., et al.: A review of deep learning for renewable energy forecasting. *Energy Convers. Manag.* 198, 111799 (2019)
22. Mosavi, A., et al.: State of the art of machine learning models in energy systems, a systematic review. *Energies* 12(7), 1301 (2019)
23. Lou, R., et al.: Application of machine learning in ocean data. In: *Multimedia Systems*, p. 3. Springer Science and Business Media Deutschland GmbH, Berlin (2021)
24. Berbić, J., et al.: Application of neural networks and support vector machine for significant wave height prediction. *Oceanologia.* 59(3), 331–349 (2017)
25. Bento, P.M.R., et al.: Ocean wave energy forecasting using optimised deep learning neural networks. *Ocean Eng.* 219, 108372 (2020)
26. Sadeghifar, T., et al.: Coastal wave height prediction using recurrent neural networks (RNNs) in the South Caspian Sea. *Mar. Geod.* 40(6), 454–465 (2017)
27. Serras, P., et al.: Combining random forests and physics-based models to forecast the electricity generated by ocean waves: A case study of the Mutriku wave farm. *Ocean Eng.* 189, 106314 (2019)
28. Kumar, N.K., Savitha, R., Al Mamun, A.: Ocean wave height prediction using ensemble of Extreme Learning Machine. *Neurocomputing* 277, 12–20 (2018)
29. Cornejo-Bueno, L., et al.: Significant wave height and energy flux estimation with a Genetic Fuzzy System for regression. *Ocean Eng.* 160, 33–44 (2018)
30. Cornejo-Bueno, L., et al.: Significant wave height and energy flux prediction for marine energy applications: A grouping genetic algorithm – Extreme Learning Machine approach. *Renewable Energy* 97, 380–389 (2016)
31. Oh, J., Suh, K.-D.: Real-time forecasting of wave heights using EOF – wavelet – neural network hybrid model. *Ocean Eng.* 150, 48–59 (2018)
32. Pirhooshyaran, M., Snyder, L.V.: Forecasting, hindcasting and feature selection of ocean waves via recurrent and sequence-to-sequence networks. *Ocean Eng.* 207, 107424 (2020)
33. Lou, R., et al.: Prediction of ocean wave height suitable for ship autopilot. *IEEE Trans. Intell. Transp. Syst.* 1–10, (2021)
34. Izquierdo, P., et al.: A comparison of sea-state parameters from nautical radar images and buoy data. *Ocean Eng.* 31(17–18), 2209–2225 (2004)
35. Pastor, J., Liu, Y.: Wave climate resource analysis based on a revised gamma spectrum for wave energy conversion technology. *Sustainability* 8(12), 1321 (2016)
36. Reikard, G., Pinson, P., Bidlot, J.-R.: Forecasting ocean wave energy: The ECMWF wave model and time series methods. *Ocean Eng.* 38(10), 1089–1099 (2011)
37. Shaheen, F., Verma, B., Asafuddoula, M.: Impact of automatic feature extraction in deep learning architecture. In: *2016 International Conference on Digital Image Computing: Techniques and Applications, DICTA 2016*. IEEE, Piscataway, NJ (2016)
38. Nosratabadi, S., et al.: Data science in economics: Comprehensive review of advanced machine learning and deep learning methods. *Mathematics* 8, 1–25 (2020)
39. Wang, C., et al.: Kervolutional neural networks. In: *Proceedings of the IEEE Computer Society Conference on Computer Vision and Pattern Recognition*, pp 31–40. IEEE, Piscataway, NJ (2019)
40. Luo, Z., et al.: Can we forecast daily oil futures prices? Experimental evidence from convolutional neural networks. *J. Risk Financ. Manag.* 12(1), 9 (2019)
41. Mosavi, A., et al.: Comprehensive review of deep reinforcement learning methods and applications in economics. *Mathematics.* 8(10), 1640 (2020)
42. Mitiche, I., et al.: 1D-CNN based real-time fault detection system for power asset diagnostics. *IET Gener. Transm. Distrib.* 14(24), 5766–5773 (2020)
43. Bento, P., et al.: Short-term load forecasting using optimized LSTM networks via improved bat algorithm. In: *2018 International Conference on Intelligent Systems*, pp. 351–357. IEEE, Piscataway, NJ (2018)

**How to cite this article:** Bento P, et al.: Ocean wave power forecasting using convolutional neural networks. *IET Renew. Power Gener.* 15:3341–3353. (2021). <https://doi.org/10.1049/rpg2.12258>.

## APPENDIX

As mentioned in Section 4, the results regarding the best forecasting errors for each buoy and forecasting horizon, that is, the maximum value in terms of  $r$  and the minimum values in terms of  $MAPE \log (\%)$  and  $RMSE$ , Tables A.1–A.3, are here provided. Also, the box and whisker plots displaying the error metrics distribution for datasets 42056 and 44014, considering all horizons, is shown in Figure A.1 and A.2. Last of all, the results from the direct comparative analysis of the different ML techniques using the same input data can be seen in Tables A.4–A.6.

**TABLE A.1** Forecasting errors: Buoy 41048 (best values)

For hor/season	Winter Week			Spring Week			Summer Week			Fall Week		
	$r$	MAPElog	RMSE	$r$	MAPElog	RMSE	$r$	MAPElog	RMSE	$r$	MAPElog	RMSE
1 h	0.97	13.02	5.75	0.96	13.60	4.21	0.96	14.08	2.68	0.97	10.30	2.80
2 h	0.95	16.38	7.17	0.96	15.08	3.85	0.94	15.86	3.08	0.96	11.65	3.62
3 h	0.94	20.04	8.41	0.93	17.60	4.13	0.91	18.73	3.55	0.95	13.67	4.17
6 h	0.94	27.22	8.28	0.78	24.53	5.47	0.85	29.30	4.82	0.88	24.34	6.99
12 h	0.87	35.65	10.82	0.34	49.88	11.40	0.79	37.05	6.10	0.61	46.35	18.35

**TABLE A.2** Forecasting errors: Buoy 42056 (best values)

For hor/season	Winter Week			Spring Week			Summer Week			Fall Week		
	$r$	MAPElog	RMSE	$r$	MAPElog	RMSE	$r$	MAPElog	RMSE	$r$	MAPElog	RMSE
1 h	0.97	9.04	0.73	0.95	8.87	0.25	0.97	9.57	0.24	0.95	11.05	2.29
2 h	0.96	11.51	0.89	0.94	11.47	0.31	0.96	11.28	0.29	0.94	14.19	2.53
3 h	0.94	14.68	1.03	0.91	13.89	0.36	0.96	11.60	0.32	0.91	17.49	3.06
6 h	0.89	20.22	1.34	0.78	22.24	0.64	0.90	21.27	0.57	0.85	24.69	4.22
12 h	0.73	29.53	2.01	0.52	39.34	1.58	0.89	19.80	0.56	0.73	37.42	6.44

**TABLE A.3** Forecasting errors: Buoy 44014 (best values)

For hor/season	Winter Week			Spring Week			Summer Week			Fall Week		
	$r$	MAPElog	RMSE	$r$	MAPElog	RMSE	$r$	MAPElog	RMSE	$r$	MAPElog	RMSE
1 h	0.97	12.71	4.51	0.98	17.60	11.94	0.93	13.71	0.39	0.94	17.45	3.43
2 h	0.96	16.62	5.44	0.94	23.67	16.86	0.88	18.80	0.50	0.90	25.07	4.62
3 h	0.95	21.74	5.50	0.95	32.72	18.64	0.80	25.06	0.63	0.87	34.48	5.34
6 h	0.88	36.75	7.53	0.90	48.56	26.07	0.61	30.37	0.85	0.75	53.07	7.93
12 h	0.72	53.19	9.51	0.86	63.40	32.40	0.49	38.29	1.08	0.53	78.45	11.88

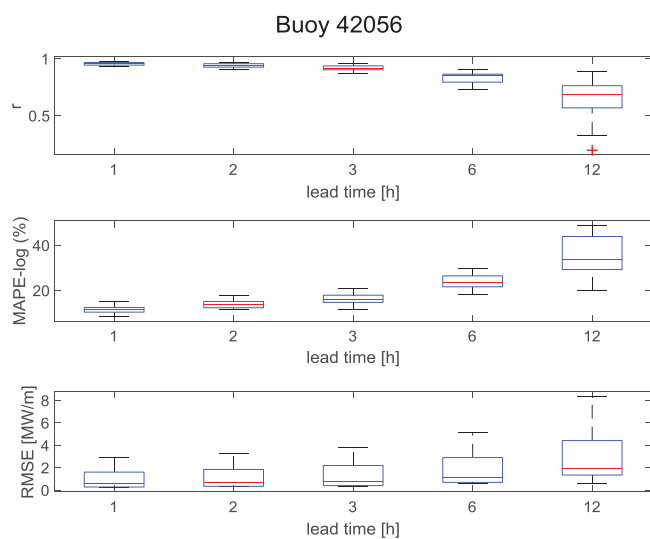
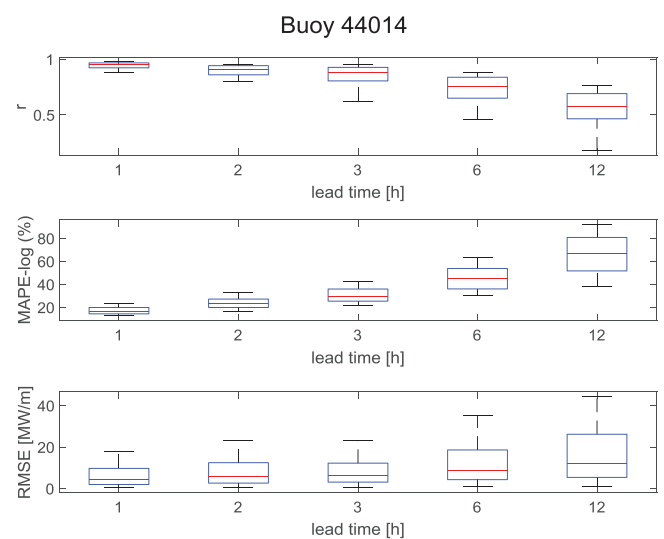
**FIGURE A.1** Box plots of the error metrics distributions, considering all forecasting horizons (buoy 42056)**FIGURE A.2** Box plots of the error metrics distributions, considering all forecasting horizons (buoy 44014)

TABLE A.4 Forecasting errors comparison: Buoy 41048 (mean results)

41048 <i>r</i>	Winter Week				Spring Week				Summer Week				Fall Week			
	NN	RBNN	SVR	CNN	NN	RBNN	SVR	CNN	NN	RBNN	SVR	CNN	NN	RBNN	SVR	CNN
1 h	0.86	0.95	0.95	<b>0.96</b>	0.86	0.94	<b>0.95</b>	<b>0.95</b>	0.86	0.92	0.83	<b>0.94</b>	0.91	0.92	0.96	<b>0.97</b>
2 h	0.81	0.91	0.90	<b>0.95</b>	0.77	0.91	0.93	<b>0.94</b>	0.89	0.89	0.64	<b>0.92</b>	0.88	0.89	0.93	<b>0.95</b>
3 h	0.82	0.88	0.86	<b>0.93</b>	0.77	0.87	0.88	<b>0.92</b>	0.86	0.86	0.36	<b>0.89</b>	0.84	0.89	<b>0.92</b>	<b>0.92</b>
6 h	0.72	0.73	0.79	<b>0.92</b>	0.63	0.67	0.65	<b>0.72</b>	0.81	<b>0.82</b>	0.34	0.80	0.74	0.72	0.79	<b>0.82</b>
12 h	0.60	0.62	0.73	<b>0.85</b>	<b>0.35</b>	0.09	0.14	0.29	0.63	<b>0.70</b>	0.12	0.69	0.51	0.48	0.45	<b>0.54</b>
<b>MAPE-log</b>	<b>NN</b>	<b>RBNN</b>	<b>SVR</b>	<b>CNN</b>	<b>NN</b>	<b>RBNN</b>	<b>SVR</b>	<b>CNN</b>	<b>NN</b>	<b>RBNN</b>	<b>SVR</b>	<b>CNN</b>	<b>NN</b>	<b>RBNN</b>	<b>SVR</b>	<b>CNN</b>
1 h	42.6	17.5	17.7	<b>14.4</b>	49.5	18.6	19.1	<b>14.3</b>	18.0	16.3	22.5	<b>15.5</b>	26.3	14.2	22.4	<b>11.1</b>
2 h	46.0	21.2	25.6	<b>17.6</b>	96.3	21.5	21.2	<b>16.1</b>	23.0	18.1	27.7	<b>17.8</b>	24.9	17.9	21.0	<b>14.0</b>
3 h	35.2	25.3	36.3	<b>21.5</b>	77.8	26.5	28.5	<b>18.8</b>	28.7	20.5	33.5	<b>20.3</b>	28.9	18.8	25.2	<b>17.2</b>
6 h	56.2	38.3	44.4	<b>28.2</b>	63.5	38.7	47.0	<b>28.3</b>	38.9	<b>25.3</b>	38.5	33.3	36.7	<b>31.1</b>	33.9	31.7
12 h	65.5	42.7	59.8	<b>38.9</b>	55.6	57.8	88.9	<b>52.8</b>	54.0	<b>36.9</b>	75.4	39.0	<b>49.3</b>	51.1	56.3	51.8
<b>RMSE</b>	<b>NN</b>	<b>RBNN</b>	<b>SVR</b>	<b>CNN</b>	<b>NN</b>	<b>RBNN</b>	<b>SVR</b>	<b>CNN</b>	<b>NN</b>	<b>RBNN</b>	<b>SVR</b>	<b>CNN</b>	<b>NN</b>	<b>RBNN</b>	<b>SVR</b>	<b>CNN</b>
1 h	14.7	7.1	7.2	<b>6.2</b>	11.9	7.2	7.4	<b>4.5</b>	4.4	4.1	6.8	<b>3.0</b>	5.2	4.8	3.9	<b>3.2</b>
2 h	14.7	9.5	10.5	<b>8.1</b>	19.7	9.3	9.7	<b>4.2</b>	4.1	4.5	12.2	<b>3.4</b>	6.8	6.0	4.9	<b>3.9</b>
3 h	16.2	10.9	13.9	<b>9.4</b>	14.7	10.6	8.7	<b>5.2</b>	5.1	5.1	11.1	<b>4.0</b>	9.0	5.7	5.5	<b>4.9</b>
6 h	23.4	15.3	13.9	<b>8.9</b>	18.5	12.2	14.1	<b>6.4</b>	<b>5.5</b>	<b>5.5</b>	11.8	5.7	10.9	10.5	9.2	<b>8.4</b>
12 h	24.4	16.5	16.8	<b>12.3</b>	20.5	17.4	21.0	<b>12.7</b>	7.6	7.0	14.0	<b>6.9</b>	21.2	21.7	21.7	<b>19.7</b>

TABLE A.5 Forecasting errors comparison: Buoy 42056 (mean results)

42056 <i>r</i>	Winter Week				Spring Week				Summer Week				Fall Week			
	NN	RBNN	SVR	CNN	NN	RBNN	SVR	CNN	NN	RBNN	SVR	CNN	NN	RBNN	SVR	CNN
1 h	0.96	0.95	0.96	<b>0.97</b>	0.90	0.93	0.89	<b>0.95</b>	0.90	0.95	0.93	<b>0.97</b>	0.92	0.91	0.93	<b>0.94</b>
2 h	0.94	0.93	0.94	<b>0.95</b>	0.88	0.91	0.87	<b>0.93</b>	0.91	<b>0.95</b>	0.92	<b>0.95</b>	0.82	0.90	0.90	<b>0.93</b>
3 h	0.88	0.92	0.90	<b>0.93</b>	0.88	0.88	0.78	<b>0.90</b>	0.91	<b>0.95</b>	0.90	<b>0.95</b>	0.86	0.88	0.88	<b>0.90</b>
6 h	<b>0.87</b>	<b>0.87</b>	<b>0.87</b>	<b>0.87</b>	0.71	0.72	0.66	<b>0.75</b>	0.87	<b>0.93</b>	0.86	0.87	0.78	0.82	0.79	<b>0.84</b>
12 h	<b>0.68</b>	0.66	0.60	0.67	0.46	<b>0.51</b>	0.37	0.40	0.64	<b>0.90</b>	0.70	0.84	0.70	<b>0.75</b>	0.70	0.69
<b>MAPE-log</b>	<b>NN</b>	<b>RBNN</b>	<b>SVR</b>	<b>CNN</b>	<b>NN</b>	<b>RBNN</b>	<b>SVR</b>	<b>CNN</b>	<b>NN</b>	<b>RBNN</b>	<b>SVR</b>	<b>CNN</b>	<b>NN</b>	<b>RBNN</b>	<b>SVR</b>	<b>CNN</b>
1 h	13.3	12.6	12.4	<b>10.1</b>	22.2	17.2	20.7	<b>10.1</b>	27.2	16.5	23.8	<b>12.3</b>	14.1	14.4	12.8	<b>12.2</b>
2 h	14.2	14.1	14.7	<b>12.9</b>	18.2	19.2	21.8	<b>12.7</b>	33.0	16.4	22.7	<b>15.6</b>	73.3	16.8	15.8	<b>15.4</b>
3 h	24.4	<b>15.9</b>	19.2	16.0	17.6	21.2	31.2	<b>15.4</b>	24.0	16.7	43.2	<b>14.7</b>	35.7	19.4	19.0	<b>18.7</b>
6 h	23.1	<b>21.7</b>	23.3	22.3	25.1	28.1	38.2	<b>24.7</b>	37.4	<b>17.8</b>	43.4	27.5	46.6	28.7	29.5	<b>26.9</b>
12 h	33.1	33.6	34.7	<b>31.6</b>	43.1	<b>39.7</b>	59.3	45.1	58.9	<b>21.3</b>	53.6	24.2	44.4	42.1	38.1	41.8
<b>RMSE</b>	<b>NN</b>	<b>RBNN</b>	<b>SVR</b>	<b>CNN</b>	<b>NN</b>	<b>RBNN</b>	<b>SVR</b>	<b>CNN</b>	<b>NN</b>	<b>RBNN</b>	<b>SVR</b>	<b>CNN</b>	<b>NN</b>	<b>RBNN</b>	<b>SVR</b>	<b>CNN</b>
1 h	0.90	0.91	0.83	<b>0.78</b>	0.59	0.38	0.42	<b>0.27</b>	0.54	0.33	0.39	<b>0.27</b>	2.87	3.19	2.70	<b>2.52</b>
2 h	1.03	1.05	1.01	<b>0.95</b>	0.52	0.42	0.50	<b>0.34</b>	0.66	0.31	0.38	<b>0.34</b>	6.15	3.61	3.42	<b>2.85</b>
3 h	1.44	1.17	1.28	<b>1.13</b>	0.49	0.47	0.61	<b>0.42</b>	0.52	0.32	0.47	0.39	4.79	4.18	3.72	<b>3.37</b>
6 h	1.49	1.46	1.49	1.47	0.78	0.71	0.88	<b>0.69</b>	0.89	<b>0.37</b>	0.53	0.67	5.76	5.48	5.35	<b>4.61</b>
12 h	2.26	2.32	2.41	<b>2.21</b>	1.69	<b>1.52</b>	1.97	1.70	2.01	<b>0.50</b>	0.81	0.78	7.43	7.41	<b>6.74</b>	7.02

**TABLE A.6** Forecasting errors comparison: Buoy 44014 (mean results)

44014	Winter Week				Spring Week				Summer Week				Fall Week			
	NN	RBNN	SVR	CNN	NN	RBNN	SVR	CNN	NN	RBNN	SVR	CNN	NN	RBNN	SVR	CNN
<i>r</i>																
1 h	0.84	0.93	0.82	<b>0.97</b>	0.81	0.89	0.31	<b>0.97</b>	0.92	0.84	0.91	<b>0.91</b>	0.93	0.91	0.93	<b>0.93</b>
2 h	0.82	0.92	0.89	<b>0.94</b>	0.74	0.88	0.40	<b>0.93</b>	0.86	0.79	0.84	<b>0.84</b>	<b>0.90</b>	0.85	0.90	0.88
3 h	0.65	0.88	0.61	<b>0.93</b>	0.80	0.87	0.13	<b>0.93</b>	0.75	0.69	0.67	<b>0.73</b>	0.83	0.76	<b>0.87</b>	0.84
6 h	0.59	0.82	0.30	<b>0.84</b>	0.65	0.83	0.35	<b>0.86</b>	0.49	<b>0.53</b>	0.36	<b>0.53</b>	0.62	0.50	0.70	<b>0.72</b>
12 h	0.52	0.65	-0.30	<b>0.68</b>	0.55	0.73	0.18	<b>0.80</b>	0.32	<b>0.45</b>	0.27	0.41	0.39	0.16	0.36	<b>0.51</b>
<b>MAPE-log</b>	<b>NN</b>	<b>RBNN</b>	<b>SVR</b>	<b>CNN</b>	<b>NN</b>	<b>RBNN</b>	<b>SVR</b>	<b>CNN</b>	<b>NN</b>	<b>RBNN</b>	<b>SVR</b>	<b>CNN</b>	<b>NN</b>	<b>RBNN</b>	<b>SVR</b>	<b>CNN</b>
1 h	22.4	18.7	19.1	<b>13.8</b>	68.4	28.7	49.2	<b>19.2</b>	18.4	26.1	16.1	<b>15.8</b>	31.4	26.6	37.7	<b>21.5</b>
2 h	107.4	22.0	21.9	<b>18.6</b>	50.7	33.1	58.4	<b>26.1</b>	21.9	27.9	23.6	<b>21.7</b>	37.4	34.0	33.0	<b>29.0</b>
3 h	133.1	26.8	30.7	<b>23.6</b>	54.7	36.8	68.5	<b>35.1</b>	26.1	30.1	31.6	<b>26.8</b>	46.3	42.4	66.4	<b>39.0</b>
6 h	95.7	<b>39.4</b>	55.0	39.5	92.3	<b>51.2</b>	94.6	52.2	32.3	36.5	39.8	<b>33.3</b>	74.7	63.8	70.9	<b>57.2</b>
12 h	114.0	<b>54.0</b>	81.4	57.9	113.4	<b>63.9</b>	130.0	68.8	39.1	<b>42.9</b>	44.0	43.3	104.7	94.8	97.5	<b>84.9</b>
<b>RMSE</b>	<b>NN</b>	<b>RBNN</b>	<b>SVR</b>	<b>CNN</b>	<b>NN</b>	<b>RBNN</b>	<b>SVR</b>	<b>CNN</b>	<b>NN</b>	<b>RBNN</b>	<b>SVR</b>	<b>CNN</b>	<b>NN</b>	<b>RBNN</b>	<b>SVR</b>	<b>CNN</b>
1 h	12.6	9.8	12.2	<b>5.8</b>	33.2	31.1	98.8	<b>15.0</b>	0.4	0.6	0.4	<b>0.4</b>	<b>3.7</b>	4.1	<b>3.7</b>	<b>3.7</b>
2 h	17.8	9.2	11.6	<b>6.6</b>	37.1	32.6	73.5	<b>18.2</b>	0.6	0.7	0.6	<b>0.6</b>	<b>4.8</b>	5.6	<b>4.8</b>	5.0
3 h	19.5	10.9	16.4	<b>6.7</b>	35.0	31.6	118.5	<b>20.5</b>	0.7	0.8	0.9	<b>0.7</b>	6.4	7.4	<b>5.6</b>	5.9
6 h	17.6	10.3	22.6	<b>8.9</b>	40.5	34.4	249.2	<b>28.9</b>	1.0	<b>0.9</b>	1.3	1.0	10.5	11.2	9.1	<b>8.6</b>
12 h	23.7	14.5	41.0	<b>10.6</b>	44.7	39.4	229.5	<b>36.1</b>	1.2	<b>1.0</b>	1.3	1.2	17.5	19.3	16.7	<b>12.9</b>